AIP | Applied Physics Letters

Edge-induced flattening in the fabrication of ultrathin freestanding crystalline silicon sheets

Gokul Gopalakrishnan, David A. Czaplewski, Kyle M. McElhinny, Martin V. Holt, Juan C. Silva-Martínez et al.

Citation: Appl. Phys. Lett. **102**, 033113 (2013); doi: 10.1063/1.4789553
View online: http://dx.doi.org/10.1063/1.4789553
View Table of Contents: http://apl.aip.org/resource/1/APPLAB/v102/i3
Published by the American Institute of Physics.

Related Articles

Relaxation of biofunctionalized magnetic nanoparticles in ultra-low magnetic fields
J. Appl. Phys. 113, 043911 (2013)

Surface enhanced fluorescence and Raman scattering by gold nanoparticle dimers and trimers
J. Appl. Phys. 113, 033102 (2013)

Formation of Si or Ge nanodots in Si3N4 with in-situ donor modulation doping of adjacent barrier material
AIP Advances 3, 012109 (2013)

Pressure effect on ZnO nanoparticles prepared via laser ablation in water
J. Appl. Phys. 113, 033509 (2013)

A microscopic study of strongly plasmonic Au and Ag island thin films
J. Appl. Phys. 113, 034302 (2013)

Additional information on Appl. Phys. Lett.

Journal Homepage: http://apl.aip.org/
Journal Information: http://apl.aip.org/about/about_the_journal
Top downloads: http://apl.aip.org/features/most_downloaded
Information for Authors: http://apl.aip.org/authors

ADVERTISEMENT

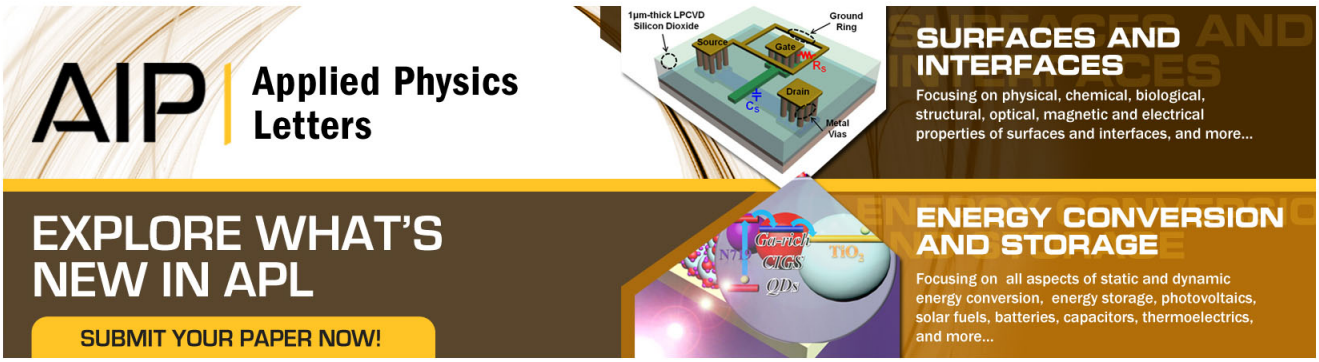

Edge-induced flattening in the fabrication of ultrathin freestanding crystalline silicon sheets

Gokul Gopalakrishnan,[1,a)] David A. Czaplewski,[2] Kyle M. McElhinny,[1] Martin V. Holt,[2] Juan C. Silva-Martínez,[1,3] and Paul G. Evans[1,b)]
[1]*Materials Science and Engineering and Materials Science Program, University of Wisconsin, Madison, Wisconsin 53706, USA*
[2]*Center for Nanoscale Materials, Argonne National Laboratory, Argonne, Illinois 60439, USA*
[3]*Department of Chemical Engineering, University of Puerto Rico-Mayagüez Campus, Mayagüez, Puerto Rico 00681-9000, Puerto Rico*

(Received 5 October 2012; accepted 10 January 2013; published online 25 January 2013)

Silicon nanomembranes are suspended single-crystal sheets of silicon, tens of nanometers thick, with areas in the thousands of square micrometers. Challenges in fabrication arise from buckling due to strains of over 10^{-3} in the silicon-on-insulator starting material. In equilibrium, the distortion is distributed across the entire membrane, minimizing the elastic energy with a large radius of curvature. We show that flat nanomembranes can be created using an elastically metastable configuration driven by the silicon-water surface energy. Membranes as thin as 6 nm are fabricated with vertical deviations below 10 nm in a central 100 μm × 100 μm area. © *2013 American Institute of Physics*. [http://dx.doi.org/10.1063/1.4789553]

Freestanding nanomembranes provide an ideal system for studying the physics of nanoscale crystalline materials as well as a unique way to create new functionalities. Among inorganic membrane materials, silicon nanomembranes display a range of unusual properties not seen in the bulk, including reduced thermal conductivity and giant persistent photoconduction.[1–3] Membranes that are flat, exhibiting a minimal curvature of the lattice planes, can be used in studies of phonon confinement via diffuse x-ray scattering and in other experiments that require crystallographically uniform volumes.[4,5] In such measurements, flat crystalline nanomembranes with large lateral extents are needed in order to resolve weak scattering signals. Fabrication of such membranes has been successful in metallic systems,[6,7] but has proven challenging in semiconductors like silicon. Freestanding silicon membranes have applications in electronic and photonic materials,[8–11] micromechanical devices,[12–16] x-ray optics,[17–19] macromolecular filters,[20] lithographic templates,[17,19] as sensors,[21,22] and as low-absorption supports in transmission electron microscopy. All of these applications benefit from flat crystalline structures with low lateral inhomogeneity. Ultra-thin freestanding membranes with nanometer-scale flatness, however, have not been realized. Instead, a buckling pattern is commonly observed.[1,14,15,23,24] In this letter, we show that flat Si nanomembranes can be created using a fabrication process that limits the buckling to a region near the edges of the window supporting the membrane. The membranes are placed under sufficient tension to overcome the buckling instability resulting from fabrication-induced residual strains.

By introducing the edge-induced tension, membranes can be produced with thicknesses as small as 6 nm that exhibit less than 10 nm of vertical distortion over lateral dimensions of 100 μm or more. The process begins with a silicon-on-insulator (SOI) substrate and uses an anisotropic wet etching procedure starting from a photolithographic pattern on the back of the handle wafer, similar to previous reports.[16,17,21,22,25] Edge-supported membranes are released by removing the buried oxide (BOX) layer from beneath a region of the device layer. Si membranes with a large range of thicknesses from tens of μm[18,25] to tens of nm have been fabricated using this approach.[14,16,17,19–22,24,26,27] Buckling often occurs in these structures as a result of compressive stresses in the silicon device layer. Previous attempts to create flat semiconductor membranes have used either strain relief structures[5,14,15] or the deposition of a tensile-stressor overlayer.[19,21]

The compressive strain responsible for buckling results from distortion introduced during the manufacture of the SOI structure and during subsequent processing. Until it is released, the SOI device layer is constrained by the BOX layer, making elastic relaxation of the strain impossible. In a released unsupported structure in which only the edges of the membrane are fixed, the minimum elastic energy of the initially strained silicon layer is achieved when the compressive strain is relieved through buckling across the entire membrane.[28] Forming a flat area within the membrane requires that the elastic energy be concentrated into narrow regions away from the flat area. The process of fabricating a flat membrane must reach the relatively high-energy flat state by a series of steps in which the total energy of the system is successively lowered, but in which the transformation to the uniformly buckled state remains unfavorable.

Buckling patterns for membranes fabricated using a conventional release process are shown in Figs. 1(a) and 1(b), for membranes with thicknesses of 315 nm and 60 nm, respectively. A map of the vertical displacement of the surface of the 60 nm-thick buckled membrane is shown in Fig. 1(c). The maximum vertical distortion is 7.8 μm, corresponding to a curvature of 1.5×10^{-3} μm^{-1}. The magnitude of the initial compressive strain in the device layer can be

a)Electronic mail: gokul@engr.wisc.edu.
b)Electronic mail: evans@engr.wisc.edu.

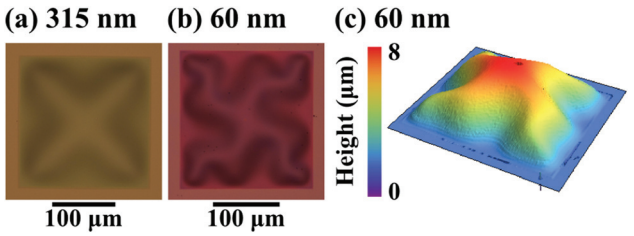

FIG. 1. Optical micrographs of buckled Si membranes with thicknesses of (a) 315 nm and (b) 60 nm. (c) Height map of the 60 nm membrane obtained by white light interferometry.

estimated by measuring the increase in the length of a line across the membrane due to elastic relaxation. For the 60 nm membrane shown in Fig. 1, the excess length along a line passing through the midpoint of the buckled membrane is 0.74 μm, which corresponds to a compressive strain of 0.37% before release. This number is comparable to an estimate for the primary buckling amplitude, A, based on a classical elastic continuum calculation, namely, $A \approx 0.5L\varepsilon^{1/2}$, where L is the edge length and ε is the device layer strain.[29] Effects consistent with the development of large compressive strains during thinning have also been observed in scanning probe microscopy studies of the roughening of SOI surfaces at high temperatures.[30]

Fig. 2(a) shows our modified membrane fabrication process creating Si-Si interfaces at the edges of the window, and thus allowing a metastable flat state to be reached. Silicon nanomembranes with thicknesses ranging from 315 nm to 6 nm were fabricated beginning with [100]-oriented SOI wafers consisting of a device layer, a BOX layer with a thickness of less than 1 μm, and a 625 μm-thick Si (100) handle wafer. The device layer was thinned by wet thermal oxidation followed by etching in hydrofluoric acid (HF). A

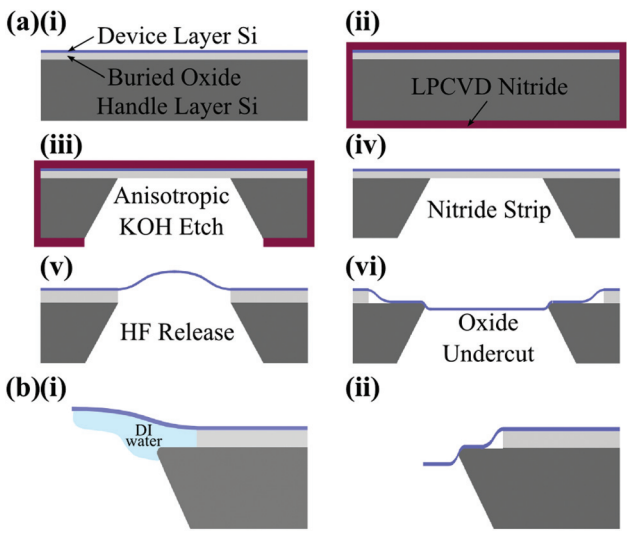

FIG. 2. (a) Fabrication of Si membranes: (i) Starting SOI structure. (ii) Protection of the device layer by SiN. (iii) Formation of windows via anisotropic etching in KOH. (iv) Removal of the SiN. (v) Release of the membrane from the buried oxide layer of SOI. (vi) Undercutting the buried oxide below the edges of the windows. (b) Flattening process during the drying of the membrane: (i) Buckled membrane at the beginning of the drying process. The trailing edge of the water film progresses outwards (to the right) from the center of the membrane as the water evaporates. (ii) Membrane profile after drying, with sharply bent regions along the inner and outer edges of the Si handle wafer surface exposed by the undercut.

200-nm-thick layer of non-stoichiometric low-stress silicon nitride (SiN) was deposited over all surfaces of the sample using low pressure chemical vapor deposition (LPCVD) at a temperature of 850 °C. The SiN layer provides a patternable mask for the subsequent etch from the back side of the wafer and also protects the device layer during further processing. Windows were patterned on the back of the SOI wafer using photolithography, and the SiN inside the patterned windows was removed by a reactive ion etch (RIE) in CF_4 + 10% O_2 at 60 mTorr. A selective anisotropic etch in KOH was performed in steps, first at 94 °C, then at 84 °C, removing the handle layer silicon from within the exposed regions. The BOX layer acted as an etch-stop for the KOH step, resulting in the formation of $SiN/Si/SiO_2$ windows with lateral dimensions of 200 μm. The SiN layer was then removed using H_3PO_4 at 160 °C.

The final step in the fabrication process is the removal of the BOX layer beneath the membrane using a 49% HF solution. This step releases membranes with thickness equal to the previously thinned SOI device layer. Flat membranes can be produced when the HF release step is conducted in a way that removes not just the BOX below the 200 μm-wide Si membrane, but also in an additional undercut region extending approximately 30 μm past the edges. The resulting configuration of the device layer, BOX, and handle wafer is shown in Fig. 2(a)(vi). After etching in HF to release the membrane and create the undercut region, the sample was cleaned in water. The risk of rupturing the membrane with forces resulting from surface tension was minimized by passing the sample through the surface of the water at an oblique angle during immersion and extraction. The undercutting and subsequent rinsing are especially valuable because these steps can be performed after the standard procedure for fabricating buckled membranes. It is, therefore, possible to apply this technique to flatten buckled nanomembranes.

This procedure generates reproducible results for membranes fabricated at two different facilities, starting from different parent SOI wafers. While a small fraction of membranes fail to flatten at the first de-wetting step following the undercut etch, a greater limitation on the yield is imposed by membrane rupture when passing the sample across a liquid surface. This failure mode gives us yields of approximately 50% in membranes thinner than 50 nm, and close to 100% for membranes thicker than 100 nm.

Optical microscopy observations immediately following removal from water show that the flattening of the released membrane occurs while the film of water on the backside of the membrane dries. The drying proceeds outwards from the center of the membrane window, as shown in schematically Fig. 2(b)(i). The creation of a flat area is favored due to the relative energies of the water-Si, air-Si, and Si-Si interfaces. The surface energy at the water-Si interface is the greatest, with a magnitude of 10^{-13} J/μm^2,[31] and its contribution is particularly large because the water-Si interface covers an area of over 10^3 μm^2 along the edges of the membrane. The receding liquid film maximizes the area of the water-Si interface and stretches the central dry portion of the membrane. The excess length in the Si membrane is thus redistributed to the wet regions near the edge (Fig. 2(b)(ii)). These wet regions are sharply curved to follow the vertical edges of the

undercut area. The elastic energy stored in curved regions at the edge of the membrane is estimated by treating the membrane edge as a beam of width w and thickness t. The beam is bent with a mean radius of curvature r, which is sensitive to surface conditions. We therefore use values of r measured by optical interferometry instead of a calculation from force balance. The strain energy from bending is proportional to $Elwt^3/r^2$, where E is the elastic modulus in flexure, and l is the length of the beam. For a 30 nm thick membrane and the experimentally observed membrane shape, the total strain energy in the edge regions is 10^{-12} J. Larger radii of curvature are observed with thicker membranes, causing the curvature and thickness dependence to partially offset each other, resulting in a weak dependence of the strain energy on the thickness of the released membranes. The energy cost for concentrating the buckling strain into a narrow region along the membrane edges is, therefore, approximately two orders of magnitude smaller than the surface energy due to wetting, of 10^{-10} J or more. The flattened state is thus favored over the uniformly buckled configuration while the membrane edges are still in contact with water.

The membrane remains in the metastable flat state after drying because the edges are constrained by the adhesive forces between the bottom of the Si membrane and the exposed surface of the Si handle wafer below the undercut region. The surface energy between the membrane and handle wafer depends on the smoothness of the contact surfaces, and thus can only be estimated. Our consideration of the energy is based on a Si-Si interface energy of 10^{-13} J/μm^2.[31] With this value, the energy released by creating the Si-Si interface is 10^{-9} J for a contact region occupying 25 μm out of a total of 30 μm length of the undercut region. The magnitude of the Si-Si interface energy is larger than the strain energy stored in the buckled Si near the edges of the membrane. We find that undercutting 30 μm of BOX, achieved with a half-hour etch in HF (Fig. 2(a)(vi)), provides surface energies large enough to ensure repeatability over a number of samples. This undercut length is observed to increase approximately linearly with etch time, in the range of 20 μm–40 μm.

Changes to the Si-Si contact energy (e.g., due to interfacial oxidation or from drying of the Si-Si contact) can lower the energy difference between the flat and uniformly buckled state. We have observed, for example, that thicker membranes relax slightly towards a buckled state over the course of one month. We have not observed such a rebuckling among thin membranes, with thicknesses near 10 nm. The relaxation is faster when membranes are vibrated during handling and measurements. However, membranes that have buckled over time may be re-flattened by repeating the final steps, with a HF dip to remove native oxide, followed by wetting in DI water and drying.

Optical images of membranes formed using the edge-induced flattening process are shown in Figs. 3(a) to 3(d). Optical profilometry of the undercut membranes reveals flat central regions over 100 μm across with height variations smaller than 10 nm. Figure 3(e) shows a height map of the 6 nm membrane acquired using white light interferometry (NewView, Zygo, Inc.), revealing narrow regions along the undercut edges where the buckling is concentrated. Figure

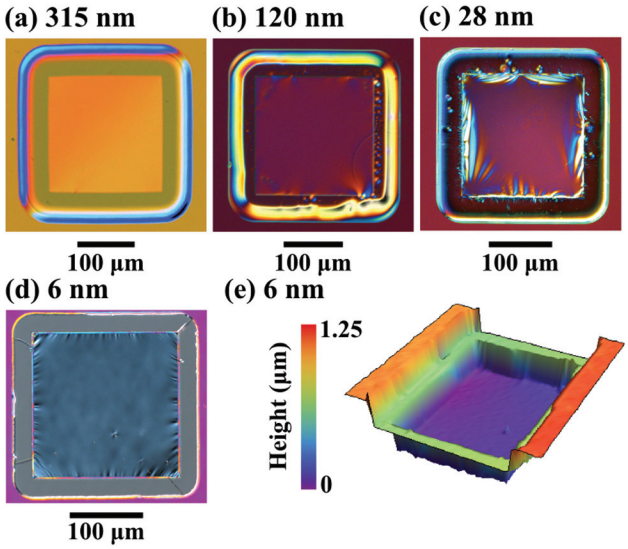

FIG. 3. (a)-(d) Optical micrographs of flat membranes fabricated via the undercut etch procedure, with thicknesses as indicated. (e) Height map of the 6 nm-thick membrane surface obtained by white light interferometry.

4(a) shows a profile of the membrane height along a line through the center of the 6 nm-thick membrane. The overall reduction in buckling can be quantified using the short- and large-scale variations in the height of the membrane within the flat region, as shown in Fig. 4(b). The curvature in a central 100 μm region of the membrane is reduced by nearly three orders of magnitude in comparison with the buckled membranes.

The crucial difference between the flat and buckled membranes is apparent in x-ray diffuse scattering measurements. Synchrotron x-ray thermal diffuse scattering (TDS) studies were conducted at station 26-ID of the advanced photon source (Argonne National Laboratory) using 10 keV photons focused to a spot size of 30 μm on the sample. Figure 5(a) shows the scattering pattern acquired using a flat 44 nm-thick membrane, in which the Si truncation rod from the (1 3 −1) reflection, as well as the TDS arising from the thermal population of phonons are visible. The details of the acquisition of the diffuse scattering patterns and the analysis of the TDS are described elsewhere.[4] In comparison, Fig. 5(b) shows the diffuse scattering acquired with a buckled 60 nm membrane. The dominant contribution to the distribution of the intensity of x-rays scattered from the buckled membrane

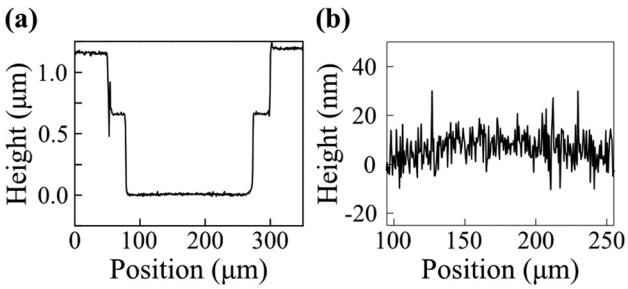

FIG. 4. (a) Height profile of the 6 nm-thick membrane along a line passing through the center of the membrane area, horizontal with respect to the micrograph in Fig. 3(d). (b) Magnified line profile along the center of the suspended membrane, showing the short- and large-scale variations in the membrane height.

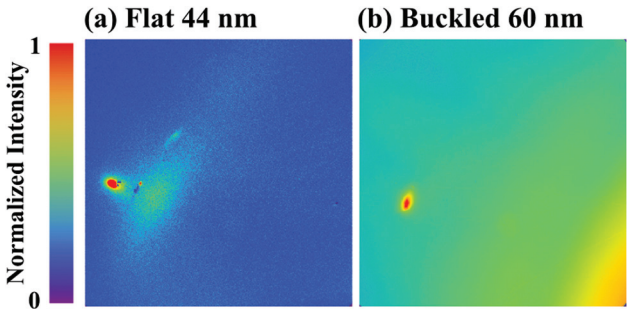

FIG. 5. X-ray diffuse scattering patterns acquired from (a) a flat 44 nm-thick membrane, and (b) a 60 nm-thick buckled membrane. The TDS signal observed with the flat membrane in (a) is small in comparison with the total intensity in (b) due to the buckling.

arises from the strain gradient and crystalline misorientations due to buckling. The TDS signal from the buckled membrane is far smaller than these static contributions to the intensity.

The fabrication strategy we describe here provides a simple approach to reduce the buckling distortion of edge-supported Si nanomembranes. The mechanism responsible for the edge-induced flattening of the membranes involves an intermediate state that uses the surface energy from contact with a liquid film to overcome the elastic energy associated with the high strain concentrations at the edges of the membrane. With this mechanism, the edge-flattening process produces thin membranes that have smaller distortions than have been previously reported. The height variation over a 100 μm region of the 6 nm membrane reported here, for example, is smaller than the height variation over a 25 μm region of a 55 nm-thick membrane fabricated using a technique aimed instead at minimizing strains in the device layer during fabrication.[22] We have demonstrated here that the flatness of the edge-flattened Si membrane reduces the static contribution to x-ray diffuse scattering, allowing experiments to probe far weaker contributions to the scattered x-ray intensity distribution than would otherwise be possible. Other probes, including optical and electron-scattering-based techniques have the potential for similar improvements with flattened membranes. Finally, differential etching will allow similar edge-flattening mechanisms to be developed, based on the scheme presented here, to create flat membranes from a number of scientifically and technologically important materials beyond Si in which similar buckling patterns have been observed, including oxides[32] and compound semiconductors.

Fabrication of nanomembranes was performed at the Wisconsin Center for Applied Microelectronics at the University of Wisconsin-Madison, and at the Center for Nanoscale Materials at Argonne National Laboratory. G.G., K.M., and P.E. acknowledge support from the US Air Force Office of Scientific Research, through Contract No. FA9550-10-1-0249. This work was performed, in part, at the Center for Nanoscale Materials, a U.S. Department of Energy, Office of Science, Office of Basic Energy Sciences user facility under Contract No. DE-AC02-06CH11357. The authors gratefully acknowledge Dr. Ralu Divan, at the Center for Nanoscale Materials, and Dr. Rob Ilic, at the Cornell Nanoscale Science and Technology Facility, for assistance with device fabrication.

[1]J. A. Rogers, M. G. Lagally, and R. G. Nuzzo, Nature **477**, 45 (2011).
[2]G. Huang and Y. Mei, Adv. Mater. **24**, 2517 (2012).
[3]J. Cuffe, E. Chavez, A. Shchepetov, P.-O. Chapuis, E. H. El Boudouti, F. Alzina, T. Kehoe, J. Gomis-Bresco, D. Dudek, Y. Pennec, B. Djafari-Rouhani, M. Prunnila, J. Ahopelto, and C. M. Sotomayor Torres, Nano Lett. **12**, 3569 (2012).
[4]G. Gopalakrishnan, M. V. Holt, K. M. McElhinny, J. W. Spalenka, D. A. Czaplewski, T. U. Schulli, and P. G. Evans, "Thermal diffuse scattering as a probe of large-wavevector phonons in nanostructures" (unpublished).
[5]G. Gopalakrishnan, M. V. Holt, K. M. McElhinny, D. A. Czaplewski, and P. G. Evans, "Probing large wavevector phonons at the nanoscale via x-ray thermal diffuse scattering," Adv. X-Anal. (accepted).
[6]Z. Jaksic and J. Matovic, Materials. **3**, 165–200 (2010).
[7]J. Matovic and Z. Jaksic, Microelectron. Eng. **86**, 906–909 (2009).
[8]M. M. Roberts, L. J. Klein, D. E. Savage, K. A. Slinker, M. Friesen, G. Celler, M. A. Eriksson, and M. G. Lagally, Nature Mater. **5**, 388 (2006).
[9]W. M. Choi, J. Z. Song, D. Y. Khang, H. Q. Jiang, Y. Y. Huang, and J. A. Rogers, Nano Lett. **7**, 1655 (2007).
[10]B. A. Fairchild, P. Olivero, S. Rubanov, A. D. Greentree, F. Waldermann, R. A. Taylor, I. Walmsley, J. M. Smith, S. Huntington, B. C. Gibson, D. N. Jamieson, and S. Prawer, Adv. Mater. **20**, 4793 (2008).
[11]S. Tomljenovic-Hanic, A. D. Greentree, C. M. de Sterke, and S. Prawer, Opt. Express **17**, 6465 (2009).
[12]B. Bercu, X. Xu, L. Montes, and P. Morfouli, Microelectron. Eng. **86**, 1303 (2009).
[13]B. Bercu, L. Montes, F. Rochette, M. Mouis, X. Xin, and P. Morfouli, Appl. Phys. Lett. **96**, 092107 (2010).
[14]E. Iwase, P. C. Hui, D. Woolf, A. W. Rodriguez, S. G. Johnson, F. Capasso, and M. Loncar, J. Micromech. Microeng. **22**, 065028 (2012).
[15]J. W. Graff and E. F. Schubert, Sens. Actuators, A **84**, 276 (2000).
[16]S. Juodkazis, Y. Nishi, H. Misawa, V. Mizeikis, O. Schecker, R. Waitz, P. Leiderer, and E. Scheer, Optics Express **17**, 15308 (2009).
[17]S. J. Utteridge, V. A. Sashin, S. A. Canney, M. J. Ford, Z. Fang, D. R. Oliver, M. Vos, and E. Weigold, Appl. Surf. Sci. **162**, 359 (2000).
[18]M. Ahn, R. K. Heilmann, and M. L. Schattenburg, J. Vac. Sci. Technol. B **25**, 2593 (2007).
[19]C. Constancias, B. Dalzotto, P. Michallon, J. Wallace, and M. Saib, J. Vac. Sci. Technol. B **28**, 194 (2010).
[20]C. C. Striemer, T. R. Gaborski, J. L. McGrath, and P. M. Fauchet, Nature **445**, 749 (2007).
[21]S. H. Lee, D. H. Kim, H. D. Yang, S. J. Kim, D. W. Shin, S. H. Woo, H. J. Lee, H. M. Seung, S. K. Lee, G. S. Lee, and J. G. Park, J. Korean Phys. Soc. **53**, 579 (2008).
[22]Z. Y. Dang, M. Motapothula, Y. S. Ow, T. Venkatesan, M. B. H. Breese, M. A. Rana, and A. Osman, Appl. Phys. Lett. **99**, 223105 (2011).
[23]K. C. Lee, J. Electrochem. Soc. **137**, 2556 (1990).
[24]C. M. Sotomayor Torres, A. Zwick, F. Poinsotte, J. Groenen, M. Prunnila, J. Ahopelto, A. Mlayah, and V. Paillard, Phys. Status Solidi C **1**, 2609 (2004).
[25]R. Iosub, C. Moldovan, and M. Modreanu, Sensor. Actuators, A **99**, 104 (2002).
[26]W. M. Vanhuffelen, M. J. Deboer, and T. M. Klapwijk, Appl. Phys. Lett. **58**, 2438 (1991).
[27]J. Groenen, F. Poinsotte, A. Zwick, C. M. Sotomayor Torres, M. Prunnila, and J. Ahopelto, Phys. Rev. B **77**, 045420 (2008).
[28]V. Ziebart, O. Paul, and H. Baltes, J. Microelectromech. Syst. **8**, 423 (1999).
[29]S. Timoshenko and J. Gere, *Theory of Elastic Stability*, 2nd ed. (Dover, New York, 2009).
[30]S. Seo, C. Euaruksakul, D. E. Savage, M. G. Lagally, and P. G. Evans, Phys. Rev. B **81**, 041302 (2010).
[31]Q. Y. Tong, R. Gafiteanu, and U. Gosele, Jpn. J. Appl. Phys., Part 1 **31**, 3483 (1992).
[32]K. Kerman, T. Tallinen, S. Ramanathan, and L. Mahadevan, J. Power Sources **222**, 359 (2013).